Chapter 2
Methodology of Seismic Tomography

Abstract In this chapter, we introduce the tomographic methods which are widely used to study three-dimensional (3-D) seismic velocity, attenuation and anisotropy structures of the Earth's interior. The fundamental mathematical equations of these methods are presented for a better understanding of the principles of seismic tomography.

Keywords Seismic tomography · Model parameterization · Ray tracing · Inversion · Resolution · Damping parameter

From seismological observations, such as P- and S-wave arrival times, amplitudes, and waveforms, basically three kinds of physical parameters can be determined to characterize the seismological structure of the Earth's interior. These parameters are seismic velocity, attenuation, and anisotropy. Applying tomographic methods to the seismological data, we can estimate the three-dimensional (3-D) distribution of these parameters, i.e., seismic velocity tomography, attenuation tomography, and anisotropy tomography. In this chapter, we introduce the general approaches to conduct the three kinds of tomographic inversions.

In general, a study of seismic tomography includes the following operations: (1) Modeling the Earth's interior structure, i.e., model parameterization; (2) Forward modeling, such as ray tracing in travel-time tomography, earthquake relocation, and the construction of observation equations; (3) Inversion, i.e., solving the large system of observation equations; and (4) Resolution and error analysis, i.e., evaluating the resolution and uncertainty of the obtained tomographic image.

2.1 Seismic Velocity Tomography

Since the advent of seismology, P- and S-wave velocities (Vp, Vs) have been the primary physical parameters to characterize the Earth's structure because they are determined mainly from P- and S-wave arrival-time data which can be measured in high quality and great quantity by the routine processing of seismic networks deployed in many regions. Hence, earthquake arrival times have been the most

© Springer Japan 2015

D. Zhao, *Multiscale Seismic Tomography,* Springer Geophysics,
DOI 10.1007/978-4-431-55360-1_2

abundant seismological data, and seismic tomography methods have been mainly applied to the arrival-time data to study the 3-D velocity structure of the Earth.

2.1.1 Model Parameterization

In the past four decades, many different approaches have been adopted to tackle the problem of imaging the Earth's interior structure. The major difference between these approaches is in the expression of the Earth's 3-D structure. Aki and Lee (1976) and Aki et al. (1977) used a number of constant-velocity blocks in three-dimensions (Fig. 2.1a); Chou and Booker (1979) adopted a velocity model with variably-sized ideal averaging volumes; Spencer and Gubbins (1980) used a 3-D analytic function defined by a small number of parameters for a velocity model; Horiuchi et al. (1982a, b) chose to use constant-velocity layers with undulating layer boundaries expressed by a power series of latitude and longitude; Thurber (1983)

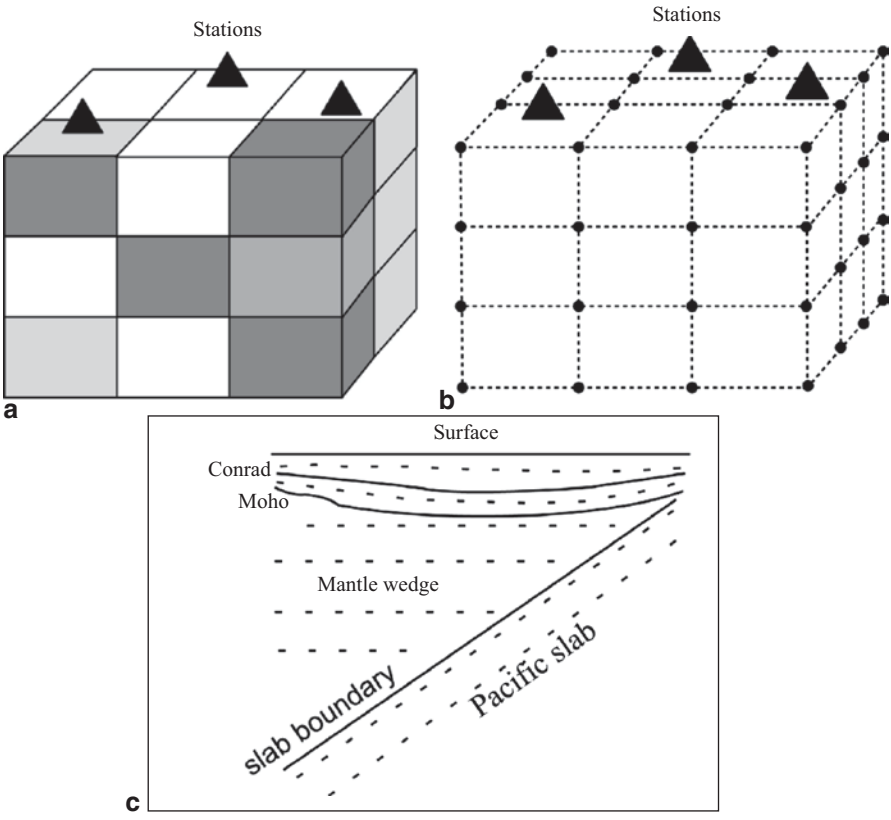

Fig. 2.1 Three ways to express the three-dimensional Earth structure (Zhao 2009). **a** The *block* approach; **b** the *grid* approach; and **c** the *boundary-grid* approach

used a 3-D grid (Fig. 2.1b); and Dziewonski (1984) adopted spherical harmonic expansions. Each of these approaches has pros and cons (for detailed reviews, see Thurber and Aki 1987; Nolet 1987, 2008; Hirahara 1990; Iyer and Hirahara 1993; Zhao 2001a, 2012).

Zhao (1991) and Zhao et al. (1992) adopted a *boundary-grid approach* to express the 3-D Earth's structure in their studies of the Japan subduction zone (Fig. 2.1c). They considered a velocity model which contains several complicated-shaped velocity discontinuities and the velocity changing in three-dimensions everywhere in the model. There are several reasons for their taking this approach. The first is that detailed studies of reflected and converted waves, as well as the first P- and S-waves, revealed the existence of the Conrad and Moho discontinuities and the upper boundary of the subducting Pacific slab beneath NE Japan (Fig. 2.1c), and the three discontinuities exhibit significant lateral depth variations (see the review by Zhao 2012). All the previous tomographic studies prior to 1990 (e.g., Aki and Lee 1976; Thurber 1983) could not handle the complex-shaped velocity discontinuities in the study area. The second reason is that clear later phases (i.e., reflected and converted waves) associated with the three discontinuities were detected in the seismograms of local crustal earthquakes and intermediate-depth earthquakes in the subducting Pacific slab (see Zhao 2012 for the detailed review). These later-phase data contain important information on the Earth's structure, in particular, in and around velocity discontinuities, hence they should be used in tomographic inversion so that local earthquakes can be better located and a better 3-D velocity model can be obtained. For this purpose, the three velocity discontinuities (i.e., the Conrad, the Moho, and the slab upper boundary) should be introduced into the 3-D velocity model. The third reason is that theoretical travel times and ray paths can be calculated much more accurately when the three discontinuities are considered in the model (Zhao 1991). Because the Pacific slab under the Japan Islands is thick (~90 km) and exhibits a higher velocity (4–6% for Vp and 6–10% for Vs) than the surrounding mantle, the slab can deviate the ray paths and travel times significantly. Introducing the Pacific slab into the model can greatly reduce the degree of non-linearity of the tomographic problem, because a better starting velocity model is adopted which is much closer to the true Earth's structure than a simple 1-D velocity model for the subduction zone. The fourth reason is that very small blocks, or grid intervals, are required to express the lateral undulations of the three discontinuities, which are impossible to realize in the actual tomographic inversion, because the available seismic stations and earthquakes are not distributed densely and uniformly enough to allow the use of small blocks, or a grid, for the tomographic inversion. Therefore, it was, and still is, the best choice to take into account the three discontinuities and the Pacific slab in the starting velocity model for the tomographic inversion (e.g., Zhao et al. 1992, 2012; Nakajima et al. 2005; Wagner et al. 2005; Huang et al. 2011a; Tian and Zhao 2012; Liu et al. 2013, 2014).

The depth distribution of a velocity discontinuity is expressed in two ways (Zhao 1991; Zhao et al. 1992). One is a continuous function such as a power series of latitude and longitude, which was used by Horiuchi et al. (1982a, b) and Zhao et al.

(1990) for estimating the Conrad and Moho geometries beneath NE Japan. The depth to the *i*th discontinuity is expressed as:

$$H_i(\phi,\lambda) = \sum\nolimits_K C_{ik} H_{ik}(\phi,\lambda) = C_{i1} + C_{i2}\phi + C_{i3}\lambda + C_{i4}\phi^2 + \cdots, \tag{2.1}$$

where φ and λ are the latitude and longitude, respectively. C_{ik} ($i=1, 2, \ldots$ m; $k=1, 2, \ldots$ n) are coefficients, m is the number of the discontinuities, and n is the number of the coefficients of the power series. Another way to express a discontinuity geometry is to use a two-dimensional (2-D) grid. When the discontinuity depth at each grid node is determined, its depth at any point (φ, λ) in the study area can be determined using a simple interpolation function:

$$Hi(\phi,\lambda) = \sum_{j=1}^{2}\sum_{k=1}^{2} h(\phi_j,\lambda_k)\left[\left(1-\left|\frac{\phi-\phi_j}{\phi_2-\phi_1}\right|\right)\left(1-\left|\frac{\lambda-\lambda_k}{\lambda_2-\lambda_1}\right|\right)\right], \tag{2.2}$$

where ϕ_j and λ_k represent the coordinates of the four grid nodes surrounding that point. The right-hand side of Eq. (2.2) is a continuous function, being a product of linear functions in ϕ and λ.

To express 3-D velocity variations in the study area, Zhao (1991) and Zhao et al. (1992) set 3-D grid nets independently for each layer bounded by two adjacent discontinuities. For each 3-D grid net within one layer, meshes of grid nodes are densely set within the layer, except for the outermost nodes which are set far away from the internal nodes so that all the seismic rays in that layer are completely covered by the grid net. The velocity (or velocity perturbation from a starting model) at each grid node is taken to be an unknown parameter except for those at the outermost nodes. The velocities at the outermost nodes are just used for the interpolation of velocities outside the modelling space. The velocity (or velocity perturbation) at any point in the *m*th layer is expressed using the following interpolation function:

$$V_m(\phi,\lambda,h) = \sum_{i=1}^{2}\sum_{j=1}^{2}\sum_{k=1}^{2} V_m(\phi_i,\lambda_j,h_k)$$

$$\cdot\left[\left(1-\left|\frac{\phi-\phi_i}{\phi_2-\phi_1}\right|\right)\left(1-\left|\frac{\lambda-\lambda_j}{\lambda_2-\lambda_1}\right|\right)\left(1-\left|\frac{h-h_k}{h_2-h_1}\right|\right)\right], \tag{2.3}$$

where h is the depth from the Earth's surface, ϕ_i, λ_j, h_k represent the coordinates of the eight grid nodes surrounding the point (φ, λ, h), and $V_m(\phi_i, \lambda_j, h_k)$ is the velocity at a grid node in the *m*th layer.

If a sufficient number of data, in particular the later-phase data associated with the discontinuities, are available, the discontinuity geometries, i.e., the coefficients C_{ik} in Eq. (2.1) or $h(\phi_j, \lambda_k)$ in Eq. (2.2), can also be taken to be unknown parameters and determined by the tomographic inversion. To obtain a stable solution, however, Zhao (1991) and Zhao et al. (1992) only considered velocities at the 3-D grid nodes in each layer to be unknown parameters, taking into account the limited number and resolution of their data. The geometries of the Conrad, the Moho and the slab upper

boundary under NE Japan obtained by previous studies were adopted, and they were fixed in the inversion process (see Zhao 1991 for details).

2.1.2 Ray Tracing

In a tomographic study, it is very important to perform 3-D ray tracing (i.e., computing travel times and ray paths in a 3-D velocity model) precisely and efficiently, because usually a great number of arrival-time data are used and ray tracing is employed several times for each datum for earthquake relocation and iterative tomographic inversions. Several exact 3-D ray tracing algorithms have been developed (e.g., Jacob 1970; Wesson 1971; Julian and Gubbins 1977; Pereyra et al. 1980), which solve the ray equation exactly and therefore require many complicated computations (CPU). Hence, these algorithms are adaptable for some forward-modeling studies, but inadequate for tomographic problems. Thurber and Ellsworth (1980) and Horie (1980) proposed separately an inexpensive scheme for computing approximate travel times by determining a precise ray path in a 1-D local approximation to the 3-D velocity structure along each ray path. Thurber (1983) introduced another approximate ray tracing technique which adopts a circular arc connecting the hypocenter and receiver to represent the ray path. The two approximate techniques work well when the epicentral distance is <50 km, whereas if the epicentral distance is greater, both the travel time and ray path computed by the two approximate techniques deviate considerably from the true solution (Miyatake 1987). Hence the two techniques are not applicable to most tomographic studies, because the seismic networks used usually have apertures greater than 50 km.

A so-called *pseudo-bending* algorithm was developed by Um and Thurber (1987) for fast 3-D ray tracing, which is described briefly in the following. After some transformations, the ray equation can be written as:

$$-\frac{\mathrm{d}^2\vec{\mathrm{r}}}{\mathrm{ds}^2}=\frac{\left[(\mathrm{grad\ V})-\frac{\mathrm{dv}}{\mathrm{ds}}\cdot\frac{\mathrm{d}\vec{\mathrm{r}}}{\mathrm{ds}}\right]}{\mathrm{V}}, \tag{2.4}$$

where $\vec{\mathrm{r}}$ is the position vector along a ray, and s is the ray length. The first term of the right-hand side of Eq. (2.4) is a velocity gradient, whereas the second term is simply the component of a velocity gradient parallel to the ray vector. Thus, Eq. (2.4) states that the component of a velocity gradient normal to the ray vector is always antiparallel to the ray path curvature. This geometric interpretation of the ray equation was first given by Cerveny et al. (1977), which was used by Um and Thurber (1987) for performing 3-D ray tracing.

Consider three adjacent points along a ray path (Fig. 2.2). Temporarily, we assume that the two end points, X_{k-1} and X_{k+1}, are fixed. A new point X'_k, instead of the previous point X_k, is sought to minimize the travel time along the ray segment from X_{k-1} to X_{k+1}. Two variables are defined for finding the new point X'_k: the

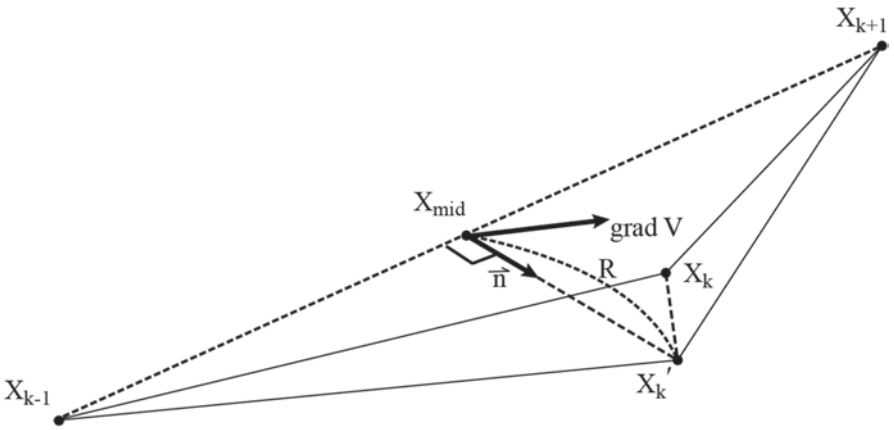

Fig. 2.2 Illustration of a three-point perturbation scheme adopted by the pseudo-bending method (Um and Thurber 1987). See the text for details

direction $\vec{n}$ and the amount R of offset from the mid-point X_{mid}. Because the local ray direction at X'_k, can be approximately expressed by the direction of the line connecting the two end points of the ray segment, X_{k-1} and X_{k-1}, the component of a velocity gradient normal to that direction defines the curvature direction, according to Eq. (2.4). Hence, this direction gives the correct offset direction at the point X'_k, which is as follows:

$$\vec{n} = (\text{grad } V) - \left[(\text{grad } V)\cdot(X_{k+1} - X_{k-1})\right]\cdot\frac{X_{k+1} - X_{k-1}}{\left|X_{k+1} - X_{k-1}\right|^2}. \tag{2.5}$$

We need to estimate the velocity at the new point X'_k, because it is unknown before the perturbation. Using a Taylor expansion of velocity at the mid-point, V_{mid}, the velocity at the new point V'_k is approximated by:

$$V'_k = V_{mid} + \left[\vec{n}\cdot(\text{grad } V)_{mid}\right]R, \tag{2.6}$$

where $(\text{grad } V)_{mid}$ is the velocity gradient at the mid-point X_{mid}. Thus, the amount of perturbation R along the direction $\vec{n}$ can be obtained by minimizing the travel time along the ray segment connecting the three points X_{k-1}, X'_k and X_{k+1}:

$$R = -\frac{CV_{mid} + 1}{4C\vec{n}\cdot(\text{grad } V)_{mid}} + \left[\frac{(CV_{mid} + 1)^2}{\left[4C\vec{n}\cdot(\text{grad } V)_{mid}\right]^2} + \frac{L^2}{2CV_{mid}}\right]^{\frac{1}{2}}, \tag{2.7}$$

where $L = \left|X_{k+1} - X_{k-1}\right|$ and $C = \left(\frac{1}{V_{k+1}} + \frac{1}{V_{k-1}}\right)/2$. For the derivation of Eq. (2.7), see Um and Thurber (1987).

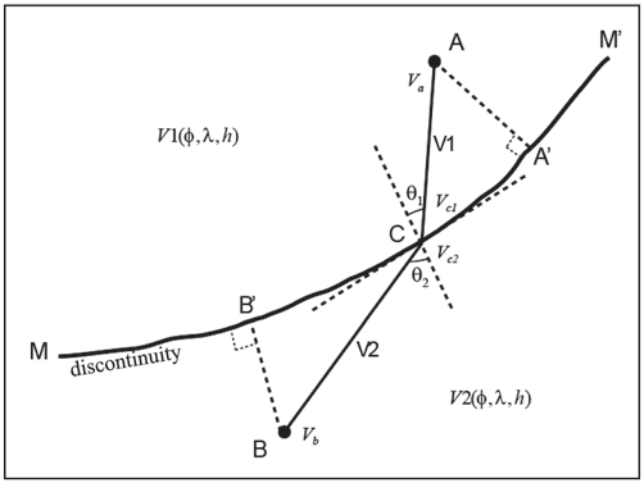

Fig. 2.3 Illustration of a scheme using Snell's law to find the intersection between a ray path A–B and a velocity discontinuity MM' (Zhao 1991; Zhao et al. 1992). See the text for details

This three-point perturbation scheme is successively extended to all the points along a ray path. The perturbation is iteratively performed until the travel time converges to a specified limit. Um and Thurber (1987) showed that the pseudo-bending scheme can find accurate travel times and ray paths in a 3-D velocity model much faster than the exact 3-D ray tracing techniques mentioned above, no matter how long the ray is. However, Um and Thurber (1987) adopted Cartesian coordinates, hence their code mainly works for a local tomography.

The pseudo-bending algorithm adopts a two-point bending approach but does not solve exactly the ray equation, and so it takes a short CPU time. However, its critical drawback is that it fails to work when a velocity discontinuity (e.g., the Moho) exists, and hence, it is applicable only to a continuous velocity model without any velocity discontinuity.

This shortcoming of the pseudo-bending scheme was overcome by Zhao (1991) and Zhao et al. (1992) in their tomographic studies of the Japan subduction zone. They proposed an algorithm that combines the pseudo-bending scheme and Snell's law to perform 3-D ray tracing in a general 3-D velocity model containing complex-shaped velocity discontinuities. Consider the case shown in Fig. 2.3. A complex-shaped velocity discontinuity, MM', exists, and the velocities on its two sides, $V_1(\phi, \lambda, h)$ and $V_2(\phi, \lambda, h)$, are continuous and change in three-dimensions. A and B are two points on different sides of MM'. Velocities at A and B are V_a and V_b, respectively. C is the intersection of a seismic ray AB and MM'. Velocities at C on the two sides of MM' are V_{c1} and V_{c2}, respectively. We take the arithmetic average V_1 of V_a and V_{c1}, and the arithmetic average V_2 of V_b and V_{c2}:

$$V_1 = \frac{V_a + V_{c1}}{2},$$
$$V_2 = \frac{V_b + V_{c2}}{2}, \tag{2.8}$$

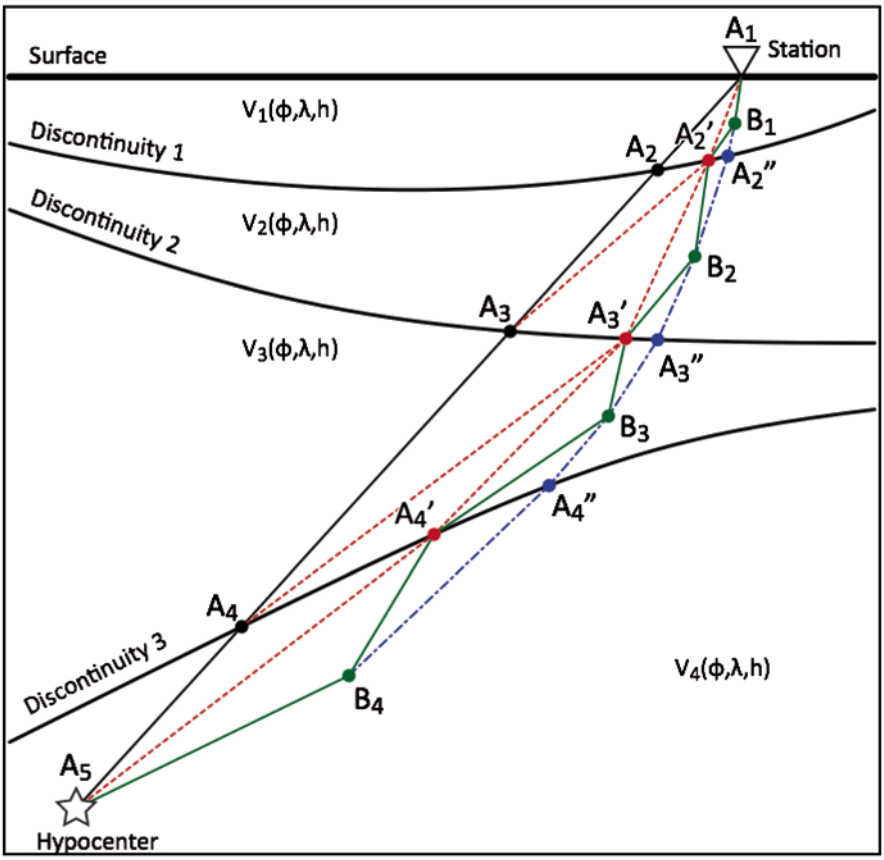

Fig. 2.4 Illustration of the 3-D ray tracing algorithm by Zhao (1991) and Zhao et al. (1992). See the text for details

to represent the mean velocities around AC and BC, respectively. This approximation is poor when A and B are far from MM', but when both A and B are close to MM' the approximation will be good enough. We then iteratively use a bisection method to find the accurate location of point C which satisfies Snell's law:

$$\frac{\sin\theta_1}{V_1} = \frac{\sin\theta_2}{V_2}. \tag{2.9}$$

Figure 2.4 shows schematically the ray tracing algorithm of Zhao (1991) and Zhao et al. (1992). For simplicity, we consider the case that three velocity discontinuities exist. The straight line A_1-A_5 connecting the station and the hypocenter is assumed to be an initial ray path. The intersections (A_2, A_3 and A_4, etc.) of the ray path with the discontinuities are called *discontinuous points* (DPs), whereas the points on the ray path between two adjacent discontinuities are called *continuous points* (CPs). The principle of the algorithm is that Snell's law is used to perturb the DPs as

described above (Fig. 2.3) and the pseudo-bending scheme is adopted to perturb the CPs (Fig. 2.2).

As shown in Fig. 2.4, we first use Snell's law to find new DPs A'_2 from A_1 and A_3, A'_3 from A'_2 and A_4, and A'4 from A'_3 and A_5. Next we use the pseudo-bending scheme to find the new CPs, viz. B_1 from A_1 and A'_2, B_2 from A'_2 and A'_3, B_3 from A'_3 and A'_4, and B_4 from A'_4 and A_5. Then, again using Snell's law, we find A''_2 from B_1 and B_2, A''_3 from B_2 and B_3, and A''_4 from B_3 and B_4, and so on. After a number of iterations the ray path converges gradually to its true location.

Zhao (1991) and Zhao et al. (1992) wrote their ray tracing code in spherical coordinates and tested the algorithm using various 3-D velocity models. They found that their code can always obtain sufficiently accurate ray paths and travel times and shorten the CPU time by one to two orders of magnitude as compared with the exact ray tracing programs. Later, Zhao (2001b, 2004) applied this 3-D ray tracing code to P, pP, PP, PcP and Pdiff phases for conducting whole-mantle tomographic inversions by considering lateral depth variations of the Moho, and the 410 and 670 km discontinuities, at a global scale (Mooney et al. 1998; Flanagen and Shearer 1998). It is found that ray paths in a 3-D global velocity model deviate considerably from those in the average 1-D model such as the iasp91 Earth model (Kennett and Engdahl 1991), and the changes in travel time and ray path amount to as much as 3.9 s and 77 km, respectively (for details, see Zhao and Lei 2004, and Chap. 7 of this book).

Several researchers have examined the algorithm of Zhao (1991) and Zhao et al. (1992) and confirmed that it is a very robust and efficient scheme for conducting ray tracing in general 3-D velocity models from local to global scales (e.g., Koketsu and Sekine 1998; Sadeghi et al. 1999; Ballard et al. 2009; Huang et al. 2013).

All the above-mentioned ray tracing methods are based on the ray theory of seismology, and they may have problems such as determining the global minimum travel-time path when multiple paths exist, and if the structure is very heterogeneous, longer CPU times and a more complex algorithm are required. To overcome these problems, some researchers have proposed wavefront-type methods (e.g., Vidale 1988, 1990; Podvin and Lecomte 1991; Coultrip 1993). In the wavefront approach, a travel-time field is constructed for the entire model space from the hypocenter, no matter how complex the structure is. This feature is an advantage of the wavefront approach, but is also its drawback. In practical applications, there are only a limited number of seismic stations in a study area. We need only travel times and ray paths from the hypocenter to the stations, and it is unnecessary to trace rays to other points in the model (Zhao 2001a). In addition, to achieve a higher accuracy, a denser 3-D grid is needed by the wavefront approach. Therefore, the larger the model is, the greater is the CPU time required.

Moser (1991) applied network theory to seismology and proposed a shortest-path method for ray tracing. Unlike in the wavefront method, Moser (1991) directly used paths between grid nodes to perform ray tracing. Although there are differences in technical details, the principles of the wavefront and the shortest-path methods are similar.

2.1.3 Inversion

Formulation of the Tomographic Problem Starting with the initial hypocenter parameters of a set of earthquakes (events), we estimate correction terms for the hypocentral and velocity structure parameters, in such a way that all the arrival-time data can be best explained in a least-squares sense. The observation equation for an arrival-time datum is written as:

$$T_{ij}^{obs} = T_{ij}^{cal} + \left(\frac{\partial T}{\partial \phi}\right)_{ij} \Delta\phi_i + \left(\frac{\partial T}{\partial \lambda}\right)_{ij} \Delta\lambda_i + \left(\frac{\partial T}{\partial h}\right)_{ij} \Delta h_i + \Delta T_{oi} + \sum_{n=1}^{N} \frac{\partial T}{\partial V_n} \Delta V_n + e_{ij}, \tag{2.10}$$

where: T_{ij}^{obs} is the observed arrival time for the *i*th event at the *j*th station;

T_{ij}^{cal} is the calculated (or theoretical) arrival time;

$\phi_i, \lambda_i, h_i, T_{oi}$ are, respectively, the latitude, longitude, focal depth and origin time of the *i*th event;

$\Delta\phi_i, \Delta\lambda_i, \Delta h_i, \Delta T_{oi}$ are the perturbations of the four hypocentral parameters;

$\left(\frac{\partial T}{\partial \phi}\right)_{ij}, \left(\frac{\partial T}{\partial \lambda}\right)_{ij}, \left(\frac{\partial T}{\partial h}\right)_{ij}$ are the partial derivatives of the travel time with respect to the hypocentral location;

$V_n, \Delta V_n$ are the velocity and its perturbation at the *n*th node of a 3-D grid arranged in the modeling space;

$\frac{\partial T}{\partial V_n}$ is the partial derivative of the travel time with respect to the velocity parameter; and

e_{ij} are higher-order terms of perturbations and error of the datum.

The theoretical travel time in Eq. (2.10) can be calculated using the above-mentioned 3-D ray tracing methods. The partial derivatives in Eq. (2.10) are calculated for the (starting) velocity model and the ray path from the hypocenter to the station determined with the 3-D ray tracing code. The partial derivatives of the travel time with respect to the hypocenter location can be written as:

$$\frac{\partial T}{\partial \phi} = -(R_0 - h)\sin i \cdot \cos \alpha / V_e,$$

$$\frac{\partial T}{\partial \lambda} = -(R_0 - h)\sin i \cdot \cos \phi \cdot \sin \alpha / V_e,$$

$$\frac{\partial T}{\partial h} = -\cos i / V_e, \tag{2.11}$$

http://www.springer.com/978-4-431-55359-5

Multiscale Seismic Tomography

Zhao, D.
2015, XV, 304 p. 146 illus., 117 illus. in color.,
Hardcover
ISBN: 978-4-431-55359-5